JOURNAL OF Materials CHEMISTRY

Sol–gel template synthesis and structural properties of a highly ordered $LiNi_{0.5}Mn_{0.5}O_2$ nanowire array

Yingke Zhou and Hulin Li*

Chemistry Department of Lanzhou University, Lanzhou 730000, People's Republic of China. Tel: +86-931-891-2517; Fax: +86-931-891-2582; E-mail: lihl@lzu.edu.cn

Received 30th August 2001, Accepted 11th December 2001
First published as an Advance Article on the web 4th February 2002

A highly ordered $LiNi_{0.5}Mn_{0.5}O_2$ nanowire array was prepared using a porous anodic aluminium oxide (AAO) template from a sol–gel solution containing Li(OAc), $Ni(OAc)_2$ and $Mn(OAc)_2$. Electron microscopy results show that $LiNi_{0.5}Mn_{0.5}O_2$ nanowires of uniform length and diameter are obtained, and that the length and diameter of the $LiNi_{0.5}Mn_{0.5}O_2$ nanowires are dependent upon the pore diameter and the thickness of the applied AAO template. X-Ray diffraction and electron diffraction investigations demonstrate that the $LiNi_{0.5}Mn_{0.5}O_2$ nanowires have a layered structure of $LiNi_{0.5}Mn_{0.5}O_2$. X-Ray photoelectron spectroscopy indicates that a nearly stoichiometric layered $LiNi_{0.5}Mn_{0.5}O_2$ material has been obtained.

1. Introduction

Many lithium intercalated transition metal oxides have been studied as the positive electrode material used in high energy density rechargeable batteries. Research work in this area has focused attention mainly on $LiMn_2O_4$ and $LiMO_2$ (M = Ni, Co) compounds synthesized by solid reaction using high temperature (HT) methods,[1–9] which show higher operating voltages than the conventional 3 V systems. These compounds crystallize in spinel-type[10] and α-$NaFeO_2$ layered structures,[11] respectively. Lithium cobaltate is one of the most advanced studied materials but has some limitations due to its high cost, moderate capacity and toxicity. Lithium nickelate is one of the most attractive materials for lithium-ion cells. However, non-stoichiometric $Li_xNi_y^{(II)}Ni_{1-y}^{(III)}O_2$ oxides are usually obtained, while nickel dioxide electrochemically formed from $LiNiO_2$ is quite active for an organic electrolyte oxidation and the reaction is exothermic. Lithiated manganese oxide, $LiMn_2O_4$, is exploited very much as a battery cathode in lithium-ion cells due to its availability and non-toxicity, in addition to its low cost compared to materials like $LiCoO_2$ and $LiNiO_2$. However, the $LiMn_2O_4$ spinel phase exhibits lower capacity and the rechargeable capacity fades rapidly for deep charge–discharge cycles, particularly at high temperature (60 °C). $LiMnO_2$ is also a candidate as a positive electrode on account of its lower cost and higher-capacity lithium-ion batteries, many attempts having been made to prepare layered $LiMnO_2$ mainly involving the use of aqueous media.[12–14] The resulting products, though interesting, have stoichiometries which differ from $LiMnO_2$, contain water or protons, are of poor crystallinity or do not maintain their structure during cycling.

A possible solution to reducing the above disadvantages is to utilize a solid solution of general formula $LiNi_{1-y}Co_yO_2$, which is isostructural with the layered oxide end-compounds and shows electrochemical features better than those of $LiNiO_2$ and $LiCoO_2$.[15–17] In this paper, we similarly prepare $LiNi_{1-y}Mn_yO_2$ solid solution in order to overcome the above disadvantages of $LiNiO_2$ and $LiMnO_2$. Moreover, efforts have been made to introduce metal dopant Mn to produce materials $Li_{1-x}Ni_{1-y}Mn_yO_2$ without a homogeneity range in the lithium content ($x \approx 0$), and doping of $LiNiO_2$ with Mn can also be used to increase the electronic conductivity and to limit the occurrence of phase transitions during the deinsertion of lithium from $Li_{1-x}NiO_2$.[18,19] In recent years, nanostructured electrode materials have attracted much interest since nanostructured Li-ion battery electrodes show better rate capabilities than conventional electrodes composed of the same materials. Better rate capabilities can be obtained because the distance over which the Li^+ must diffuse in the material is reduced dramatically in the nanostructured electrode. Moreover, the surface area of the nanostructured electrode is much greater, leading to the effective current density during charge and discharge being smaller than for a conventional electrode at the same current density. The high specific surface area of these materials has significant implications with respect to energy-storage devices based on electrochemically active sites (batteries, supercapacitors) and energy conversion devices depending on a catalytic site of defect structure (fuel cells and thermoelectric devices).[20–22] Nanostructured materials have been explored for use as cathode and anode materials in lithium-ion batteries in recent years. Novel nanostructured electrode materials provide not only good model systems for research into intercalation reactions of Li^+, but also show promise for use in some special Li-ion battery systems such as micro-batteries. As an important method for preparing nanostructured materials, the template method[23] has successfully played a crucial role in a variety of areas. Different kinds of template such as anodic porous alumina, polymer and nano-channel glass templates have been widely investigated. Normally, anodized aluminium in an appropriate acid solution forms an anodic porous alumina template. Compared with other templates, the size of the holes in the template can be readily controlled by appropriate adjustment of the anodization conditions.[24] In this paper, we report the first application of the sol–gel template method to prepare $LiNi_{0.5}Mn_{0.5}O_2$ as highly ordered array of nanowires, which produces distinctly different results when compared to conventional methods.

Sol–gel chemistry has recently evolved as a powerful approach for preparing inorganic materials such as glasses and ceramics.[25–27] This method for the synthesis of inorganic materials has a number of advantages over more conventional synthetic procedures. For example, materials of high purity can be synthesized at lower temperatures. In addition, homogeneous multicomponent systems can be obtained by mixing precursor solutions. This allows for easy chemical doping of the materials prepared. Finally, the rheological properties of the sol and the gel can be utilized in processing the material, for example, by dip coating of thin films, spinning of fibres, *etc.*[27,28] Here we have combined the concepts of sol–gel synthesis and template preparation of nanomaterials to yield a new general route for preparing $LiNi_{0.5}Mn_{0.5}O_2$ nano-arrays. This was accomplished by conducting sol–gel synthesis within the pores of various nanoporous membranes, when monodispersed nanoarrays of $LiNi_{0.5}Mn_{0.5}O_2$ nanowires were obtained. This report focuses on the fabrication process and characterization of the layered $LiNi_{0.5}Mn_{0.5}O_2$ nanowire array.

2. Experimental

2.1 Membrane preparation

High-purity aluminium sheets (99.99%, 20 mm × 10 mm) were employed in this experiment. Prior to anodization, the metal surfaces were degreased, etched in alkaline solution, rinsed in distilled water and electropolished to achieve a smooth surface. It was necessary to immerse the samples in concentrated acid or alkaline solution for several minutes to remove the oxide layer formed during the electropolishing process. All samples were rinsed in distilled water and then transferred to a nitrogen environment. The resultant clean aluminium samples were anodized at constant potential in phosphoric acid (99–101 V, 0 °C, Pt sheet as a counter electrode). Then, the whole sheet was placed into saturated $HgCl_2$ solution to separate the template membrane from the Al substrate. The membrane was rinsed with distilled water and then immersed in H_3PO_4 solution (5%) for about 30 min at 30 °C in order to dissolve the barrier-type part of nano-holes on the bottom. The AAO templates were characterized by using transmission electron microscopy (TEM) and scanning electron microscopy (SEM).

2.2 Preparation of $LiNi_{0.5}Mn_{0.5}O_2$ nanowire array

Metal acetates were used as the cationic sources, and citric acid and ethylene glycol as the monomers for forming the polymeric matrix. With a molar ratio of citric acid to LiOAc of 4 : 1, $Ni(OAc)_2$, $Mn(OAc)_2$ and LiOAc (1 : 1 : 2 molar ratio) were dissolved in a mixture of citric acid and ethylene glycol (1 : 4 molar ratio). A clear solution was produced which was heated at 140 °C to induce esterification and distill out the excess ethylene glycol. Thus the sol was obtained.

The alumina template membrane was dipped into the sol for the desired amount of time and then removed. Excess sol on the membrane surface was wiped off using a laboratory tissue, followed by drying under vacuum at 50 °C for 1 h. The membrane surface was carefully wiped again to remove salts crystallized on the surface and then heated at 600 °C for 10 h in the open air, resulting in formation of arrays of $LiNi_{0.5}Mn_{0.5}O_2$ nanowires inside the pores of the AAO template.

2.3 Characterization of $LiNi_{0.5}Mn_{0.5}O_2$ nanowire array

The structure and morphology properties of the $LiNi_{0.5}$-$Mn_{0.5}O_2$ nanowire array were characterized by several techniques. X-ray diffraction (XRD) data for the template membrane were collected using a Rigaku D/MAX2400 diffractometer with Cu-K_{α} radiation. A TEM microscope (Hitachi 600, Japan) was used to observe the morphology and degree of agglomeration of the nanowires. Prior to TEM observation, the alumina template membrane was dissolved using 3 M NaOH and then diluted with distilled water three times. SEM images were recorded with a JSM-5600LV microscope. For the SEM sample, the alumina template membrane was attached to a Cu cylinder. Then, 2 drops of 3 M NaOH were dropped onto the sample to dissolve the partial membrane, and then the samples were sputter-coated with gold before the SEM measurement in order to increase their conductivity. The X-ray photoelectron spectroscopy (XPS) data were obtained by a V. G. ESCA Lab. 2201-XL photoelectron spectrometer with a Mg Kα source, a concentric hemispherical analyser operating in fixed analyser transmission mode and a multi-channel detector. The pressure in the analysis chamber was less than 2×10^{-10} Torr. The spectra were acquired with a 50 eV pass energy and a 1 mm^2 spot (large area mode without using XL lens). The binding energy was calibrated with reference to the C 1s level of carbon (285.0 eV).

3. Results and discussion

3.1 TEM and SEM analysis

When anodized in an acidic electrolyte, aluminium forms a porous oxide with uniform and parallel pores open at one end but sealed at the other.[29–31] Its structure is described as a close-packed array of columnar cells, each containing a central pore of which the side and interval can be controlled by changing the conditions of formation.[29–31] Fig. 1(a) presents the TEM photograph of a porous AAO template with a pore diameter $d = 100 \pm 5$ nm, and a pore density of about 10^9–10^{10} cm^{-2}. Perfect hexagonal pore arrays can be observed within domains of microsize, which are separated from neighbouring aluminium oxide domains with a different orientation of the pore lattice by grain boundaries. Thus, a poly-crystalline pore structure is observed. As a further observation, the SEM photograph in Fig. 1(b) depicts the cross-section of the AAO template with pores parallel to each other and perpendicular to the surface of the membrane.

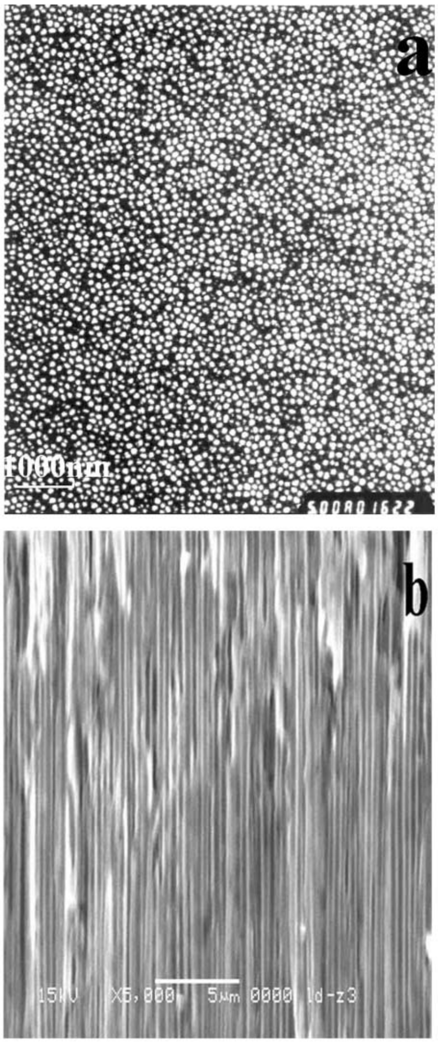

Fig. 1 (a) TEM photograph and (b) SEM photograph of AAO template.

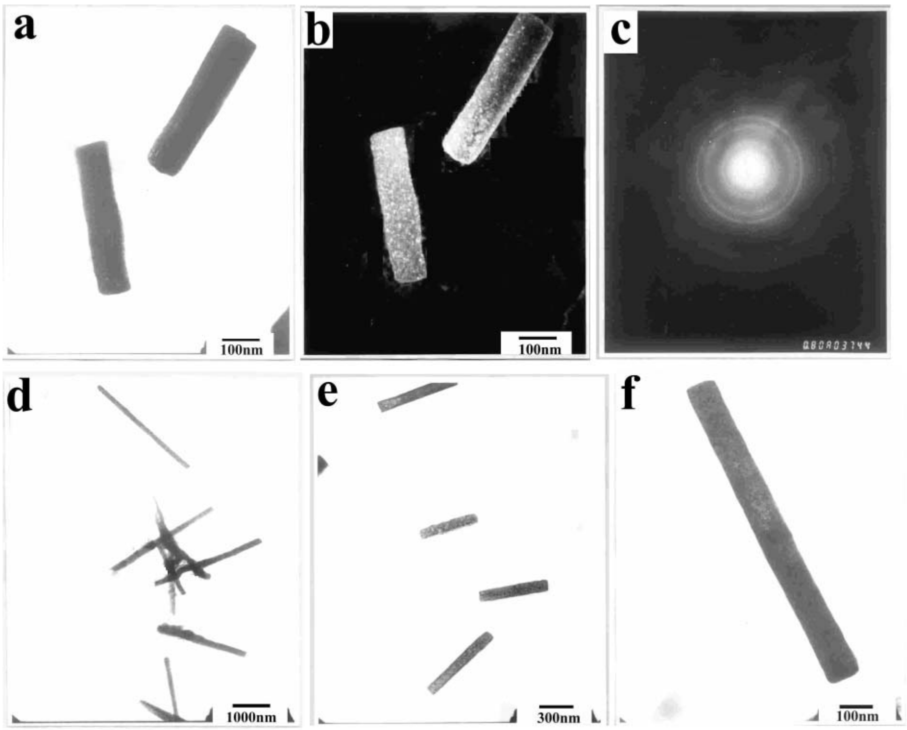

Fig. 2 TEM photographs of $LiNi_{0.5}Mn_{0.5}O_2$ nanometer wires: (a–c) The bright field TEM image, dark field TEM image and corresponding electron diffraction pattern; (d) TEM image of several $LiNi_{0.5}Mn_{0.5}O_2$ nanowires; (e, f) other TEM images of $LiNi_{0.5}Mn_{0.5}O_2$ nanowires.

TEM images of the $LiNi_{0.5}Mn_{0.5}O_2$ nanowires formed in an AAO template are shown in Fig. 2. The nanowires produced are uniformly distributed and have a diameter of around 100 nm. The length and the diameter of these nanowires correspond exactly with that of the templates. Fig. 2a and 2b show TEM images of two $LiNi_{0.5}Mn_{0.5}O_2$ nanowires at light and dark field, respectively. We can see that these images are of the same two $LiNi_{0.5}Mn_{0.5}O_2$ nanowires. There are many bright little dots in the nanowires of Fig. 2b, which indicates that the $LiNi_{0.5}Mn_{0.5}O_2$ nanowire consists of many little crystals, and that these bright crystals are exactly diffracted out from this angle when this image is taken. From this we can conclude that the $LiNi_{0.5}Mn_{0.5}O_2$ nanowire obtained in our experiment is microcrystalline. In each nanowire, the micro-crystallites are connected with each other so closely that the porosity is very low, and thus these connected structures will give good transport properties. We can also estimate the crystallite size to be about 10 nm from Fig. 2b under such conditions. The corresponding electron diffraction pattern taken from this $LiNi_{0.5}Mn_{0.5}O_2$ nanowire is shown in Fig. 2c. The diffraction spots correspond to the (003), (101), (104) and (110) diffraction planes of layered crystalline $LiNi_{0.5}Mn_{0.5}O_2$ according to the electron diffraction formula. Fig. 2d shows eight major $LiNi_{0.5}Mn_{0.5}O_2$ nanowires, of which four in the middle of the image overlap with each other, and form an irregular "#". Another two nanowires on the underside are observed only at one end, and these cross with each other. Fig. 2e shows four major $LiNi_{0.5}Mn_{0.5}O_2$ nanowires. This image shows these nanowires to have uniform length and diameter, which correspond to the pores of the AAO template employed. These nanowires are uniformly distributed, which indicates that the alumina matrix is dissolved completely. Fig. 2f shows another image of one $LiNi_{0.5}Mn_{0.5}O_2$ nanowire.

Fig. 3 shows SEM images of $LiNi_{0.5}Mn_{0.5}O_2$ nanowires grown by the AAO template. The photographs show that the nanowires are parallel with each other and few microscopic defects are found in them. Fig. 3a is a cross-section of the $LiNi_{0.5}Mn_{0.5}O_2$ nanowire array and Fig. 3b is the magnified local image of the cross-section, from which we can see the whole cross-section. These photographs show that the nanowires are parallel with each other, uniformly distributed, highly ordered and contain few microscopic defects. This is because the alumina matrix is only partially dissolved, which makes the nanowires retain their place within the pores of the nanoporous alumina matrix. Fig. 3c shows a cluster of $LiNi_{0.5}Mn_{0.5}O_2$ nanowires, of which the alumina matrix is almost dissolved completely, and only the bottoms adhere together due to the residual alumina. Both the top surface and cross-section of the $LiNi_{0.5}Mn_{0.5}O_2$ nanowire array were obtained from this image and these nanowires have a fibre-brush aspect. We can also see from it the uniform distribution and high degree of order characteristic of a nanowire array. Fig. 3d is taken at lower magnification and the visual field is larger than in Fig. 3c, and the visual fields of Fig. 3e and f are further enlarged compared to Fig. 3d. From these we find that $LiNi_{0.5}Mn_{0.5}O_2$ nanowire arrays can be produced in large areas within the pores of the AAO template. The density of the nanowires is about 4×10^9 cm^{-2} from these SEM measurements. As a result, the length of the $LiNi_{0.5}Mn_{0.5}O_2$ nanowires is equal to the thickness of the applied template, and at the same time the outside diameter of these wires is equivalent to the pore diameter of the template membrane (100 nm).

3.2 XRD analysis

The quasi-binary phase system $LiNiO_2$–$LiMnO_2$ has been reported and pure single-phase materials have been obtained for manganese contents $0\leqslant y\leqslant0.5$ in $LiNi_{1-y}Mn_yO_2$.[32] The ideal layered $LiNi_{0.5}Mn_{0.5}O_2$ has a rock salt structure with lithium and transition metal cations occupying alternate layers of octahedral sites (3a and 3b sites, respectively) in a distorted cubic close-packed oxygen ion lattice (6c site).[33–35] In space-group notation, this corresponds to the trigonal space group $R\bar{3}m$. The XRD spectrum of $LiNi_{0.5}Mn_{0.5}O_2$ nanowires within the alumina matrix is shown in Fig. 4. Although the background diffraction peaks of the Al_2O_3 template are very large, the major diffraction peaks of $LiNi_{0.5}Mn_{0.5}O_2$ are observed; these correspond closely to layered $LiNi_{0.5}Mn_{0.5}O_2$ (003), (101) and (104) planes (agreement with the JCPDS standard, card no: 16-0427). We can also see that all the diffraction-peak

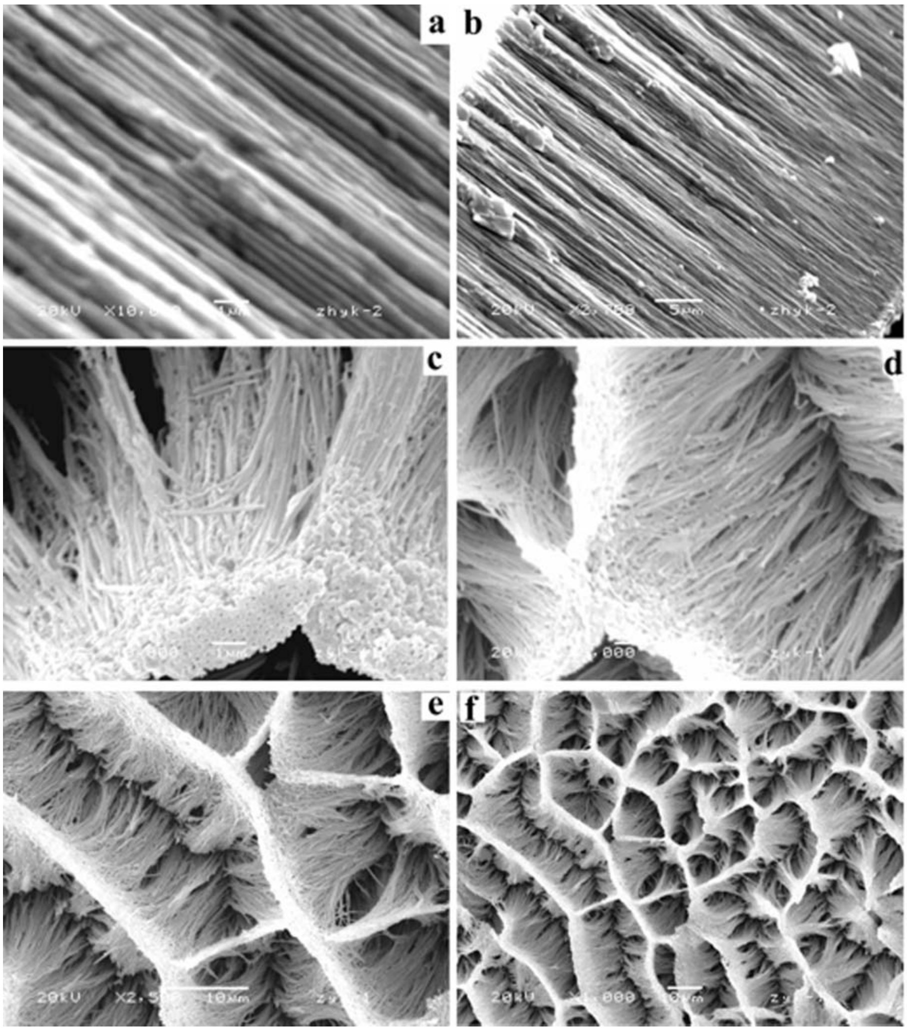

Fig. 3 SEM photographs of $LiNi_{0.5}Mn_{0.5}O_2$ nanowire arrays: (a) cross-section of $LiNi_{0.5}Mn_{0.5}O_2$ nanowire array; (b) magnified local cross-section image of $LiNi_{0.5}Mn_{0.5}O_2$ nanowire array; (c–f) other clusters of $LiNi_{0.5}Mn_{0.5}O_2$ nanowires taken at different magnifications.

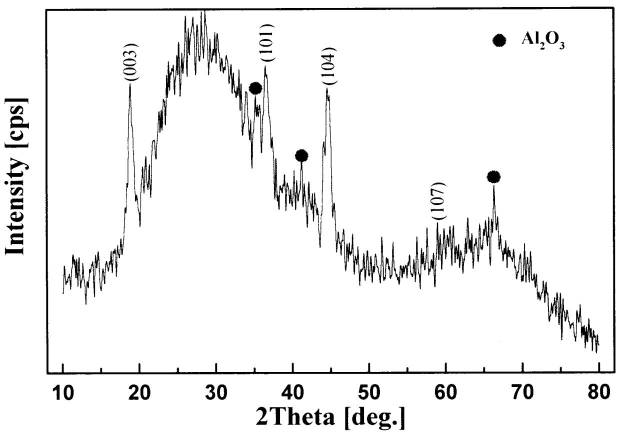

Fig. 4 XRD patterns of $LiNi_{0.5}Mn_{0.5}O_2$/alumina composite membrane.

intensities of $LiNi_{0.5}Mn_{0.5}O_2$ are smaller than those of amorphous Al_2O_3. The reason for the weaker diffraction peaks of $LiNi_{0.5}Mn_{0.5}O_2$ derives from the low concentration of $LiNi_{0.5}Mn_{0.5}O_2$ in the template and the $LiNi_{0.5}Mn_{0.5}O_2$ not being covered on the surface of the template.

3.3 XPS analysis

The chemical composition of the layered $LiNi_{0.5}Mn_{0.5}O_2$ nanowire array (within the AAO template) was obtained by XPS measurements. In an X-ray photoelectron spectroscopy (XPS) experiment, the samples are exposed to monochromic X-radiation and the properties of the inner-shell electrons are probed. Quantitative analysis of the $LiNi_{0.5}Mn_{0.5}O_2$ is made from the integrated intensities of the Ni 2p, Mn 2p and Li 1s lines, which are observed in the XPS spectrum along with peaks attributed to oxygen. Peaks corresponding to aluminium are also recorded in the spectrum. Fig 5a–e displays the XPS spectra of the Mn 2p, Ni 2p, Li 1s, O 1s and Al 2p core levels (all in excellent agreement with the standard spectra),[36] respectively, for an $LiNi_{0.5}Mn_{0.5}O_2$/AAO composite. The line of the Li 1s core level has a low intensity with a binding energy located at 53.9 eV (Fig. 5c). The line shapes of the core-level O 1s and Al 2p are Gaussian-like with binding energies of 529.6 (Fig. 5d) and 74.1 eV (Fig. 5e), respectively. We can see that the peak intensities of O 1s and Al 2p are higher than for the other elements, and this is in accord with the XRD analysis. For the quantitative analysis of O, we used the area under the O 1s peaks, bearing in mind that the part corresponding to Al_2O_3 needs to be subtracted. The peaks located at 854.3 and 871.3 eV (Fig. 5b) are attributed to the spin–orbit splitting of the Ni (2p) components, Ni ($2p_{3/2}$) and Ni ($2p_{1/2}$), respectively.[19] The entire 2p region has to be included for quantitative analysis because the total amount of the respective ion species is equal to the integral number over all the Ni (2p) states. An energy separation of 11.7 eV is observed between the Mn $2p_{3/2}$ and Mn $2p_{1/2}$ states (Fig. 5a). Thus, the Mn $2p_{3/2}$ peak in $LiNi_{0.5}Mn_{0.5}O_2$ is observed between those of MnO_2 (642.6 eV) and Mn_2O_3 (641.6 eV).[36] The intensity ratio

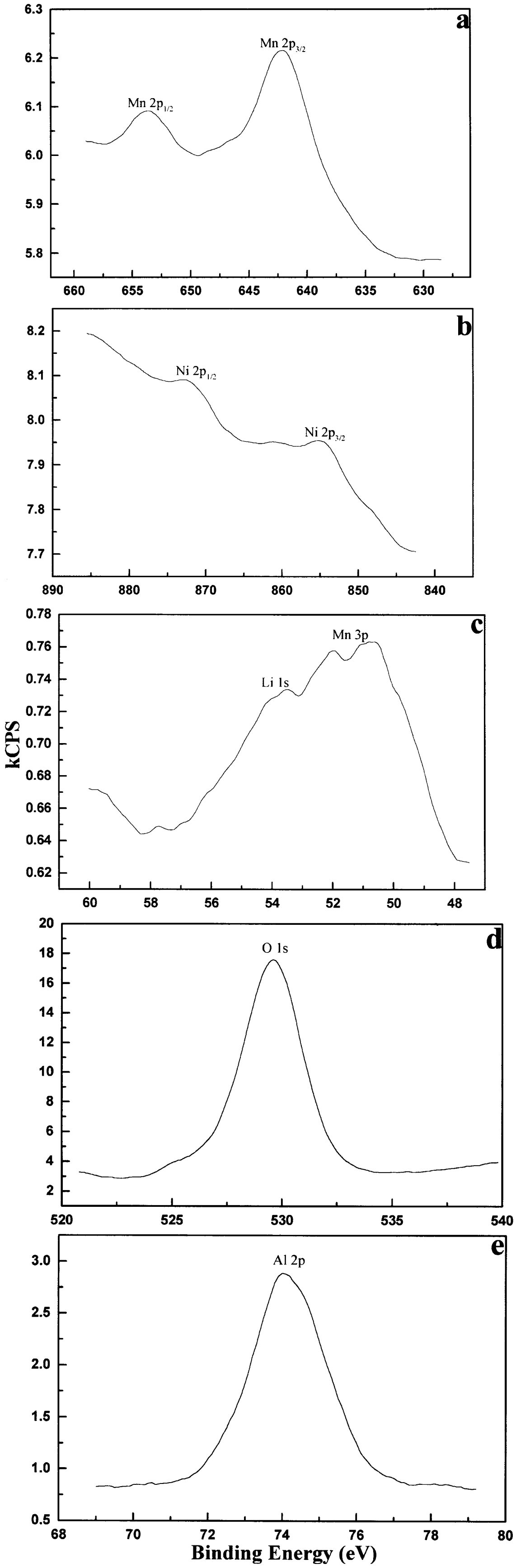

Fig. 5 XPS spectra of (a) Mn 2p; (b) Ni 2p; (c) Li 1s; (d) O 1s; and (e) Al 2p core levels for $LiNi_{0.5}Mn_{0.5}O_2$/alumina composite membrane.

between the Mn 2p, Ni 2p, Li 1s and O 1s XPS peaks (after subtraction) shows that the $LiNi_{0.5}Mn_{0.5}O_2$ product has been synthesized and closely resembles stoichiometric layered material.

4. Conclusion

An $LiNi_{0.5}Mn_{0.5}O_2$ nanowire array was successfully fabricated by a sol–gel template process. Investigations of the X-ray diffraction and electron diffraction patterns demonstrated that $LiNi_{0.5}Mn_{0.5}O_2$ nanowires have the layered structure of $LiNi_{0.5}Mn_{0.5}O_2$. Electron microscopy results show that these $LiNi_{0.5}Mn_{0.5}O_2$ nanowires have a uniform length and diameter and form a highly ordered array, the dimensions being determined by the pore diameter and the thickness of the AAO template employed. XPS analysis indicates that the nanowires closely resemble stoichiometric layered $LiNi_{0.5}Mn_{0.5}O_2$.

Acknowledgements

This work was supported by the Nation Natural Science Foundation of China (No. 69871013). We would like to express our sincere thanks to Chief Engineer Gui-Xun Cao of Gansu Instrumental Analysis & Research Center for TEM measurements and analyses, and to Chief Engineer Da-Kang Song of the Material Department of Lanzhou University for measurement and analysis of XRD data.

References

1 J. C. Hunter, *J. Solid State Chem.*, 1981, **39**, 142.
2 M. M. Thackeray, W. I. F. David, P. G. Bruce and J. B. Goodenough, *Mater. Res. Bull.*, 1983, **18**, 461.
3 J. M. Tarascon and D. Guyomard, *J. Electrochem. Soc.*, 1991, **138**, 2864.
4 T. Ohzuku, M. Kitagawa and T. Hirai, *J. Electrochem. Soc.*, 1990, **137**, 769.
5 J. M. Tarascon, D. Guyomard and G. L. Baker, *J. Power Sources*, 1993, **43–44**, 689.
6 K. Mizushina, P. C. Jones, P. J. Wiseman and J. B. Goodenough, *Mater. Res. Bull.*, 1980, **15**, 783.
7 E. Rosen, J. N. Reimers and J. R. Dahn, *Solid State Ionics*, 1993, **62**, 53.
8 P. Barboux, J. M. Tarascon and F. K. Shokoohi, *J. Solid State Chem.*, 1991, **94**, 185.
9 I. Saadoune and C. Delmas, *J. Mater. Chem.*, 1996, **6**, 193.
10 Y. Gao and J. R. Dahn, *J. Electrochem. Soc.*, 1996, **143**, 100.
11 A. Ueda and T. Ohzuku, *J. Electrochem. Soc.*, 1994, **141**, 2013.
12 M. H. Rossouw and M. M. Thackeray, *J. Solid State Chem.*, 1993, **104**, 464.
13 M. M. Thackeray, *J. Electrochem. Soc.*, 1995, **142**, 2558.
14 F. Leroux, D. Guyomard and Y. Piffard, *Solid State Ionics*, 1995, **80**, 299.
15 E. Zhecheva and R. Stoyanova, *Solid State Ionics*, 1993, **66**, 143.
16 T. Ohzuku, A. Ueda, M. Nagayama, Y. Iwakoshi and H. Komori, *Electrochim. Acta.*, 1993, **38**, 1159.
17 J. Gummow and M. M. Thackeray, *J. Electrochem. Soc.*, 1993, **140**, 3365.
18 M. E. Spahr, P. Novák, B. Schnyder, O. Haas and R. Nesper, *J. Electrochem. Soc.*, 1998, **145**, 1113.
19 B. J. Neudecker, R. A. Zuhr, B. S. Kwak and J. B. Bates, *J. Electrochem. Soc.*, 1998, **145**, 4148.
20 N. Li, C. J. Patrissi, G. Che and C. R. Martin, *J. Electrochem. Soc.*, 2000, **147**, 2044.
21 M. E. Spahr, P. S. Bitterli, R. Nesper, O. Haas and P. Novák, *J. Electrochem. Soc.*, 1999, **146**, 2780.
22 N. Li, C. R. Martin and B. Scrosati, *Electrochem.Solid-State Lett.*, 2000, **3**, 316.
23 F. Schlottif, M. Textor, U. Gerrgi and F. Roewer, *J. Mater. Sci. Lett.*, 1999, **18**, 599.
24 U. Gösele, A. P. Li, K. Nielsch, F. Muller, W. Erfurth and R. B. Wshrspohn, *Extended Abstract 196th ECS meeting*, No. 158, Toronto, Canada, May, 2000.
25 C. J. Brinker and G. W. Scherer, *Sol-Gel Science*; Academic Press; New York, 1990.
26 L. L. Hench and J. K. West, *Chem. Rev., (Washington, D.C.)*, 1990, **90**, 33.
27 M. A. Aegerter, R. C. Mehrota, I. Oehme, R. Reisfeld, S. Sakka, O. Wolfbers and C. K. Jorgensen, *Optical and Electronic Phenomena in Sol-Gel Glasses and Modern Applications*; Springer-Verlag: Berlin, 1996; **vol: 85**.

28 B. B. Lakshmi, C. J. Patrissi and C. R. Martin, *Chem. Mater.*, 1997, **9**, 2544.
29 C. A. Huber, T. E. Huber, M. Sadoqi, J. A. Lubin, S. Manalis and C. B. Prater, *Science*, 1994, **263**, 800.
30 Y. Peng, H. L. Zhang, S. L. Pan and H. L. Li, *J. Appl. Phys.*, 2000, **87**, 7405.
31 S. L. Pan, H. L. Zhang, Y. Peng, Z. Wang and H. L. Li, *Chem. J. Chin. Univ.*, 1999, **20**, 1622.
32 E. Rossen, C. D. W. Jones and J. R. Dahn, *Solid State Ionics*, 1992, **57**, 311.
33 C. Deimas and I. Saadoune, *Solid State Ionics*, 1992, **53–56** 370.
34 A. Ueda and T. Ohzuku, *Solid State Ionics*, 1994, **141**, 2010.
35 T. Ohzuku, A. Ueda, M. Nagayama, Y. lwaoshi and H. Komory, *Electrochim. Acta.*, 1993, **38**, 1159.
36 C. D. Wagner, W. M. Riggs, L. E. Davis, J. F. Moulder and G. E. Muilenberg, *Handbook of X-ray Photoelectron Spectroscopy*, Perkin-Elmer Corporation, Minnesota, December, 1978.